



Article

Assembly of ZnO Nanoparticles on SiO₂@ α -Fe₂O₃ Nanocomposites for an Efficient Photo-Fenton Reaction

Kasimayan Uma ^{1,*}, Sridharan Balu ² , Guan-Ting Pan ² and Thomas C.-K. Yang ^{1,2,*} ¹ Precision Analysis and Materials Research Center, National Taipei University of Technology, Taipei 106, Taiwan² Department of Chemical Engineering and Biotechnology, National Taipei University of Technology, Taipei 106, Taiwan; bsridharanbsc.12@gmail.com (S.B.); t6679013@gmail.com (G.-T.P.)

* Corresponding: umamahesh16@gmail.com (K.U.); ckyang@mail.ntut.edu.tw (T.C.-K.Y.)

Received: 31 July 2018; Accepted: 2 September 2018; Published: 3 September 2018



Abstract: The SiO₂@ α -Fe₂O₃/ZnO metal oxide nanocomposites employed in this study were obtained using the sol-gel method. Their photocatalytic activities were enhanced by photo-Fenton reactions. The metal oxide composite of ZnO and α -Fe₂O₃ nanoparticles were deposited on the SiO₂ nanospheres intended for visible light photocatalysis. Further, the as-synthesized SiO₂@ α -Fe₂O₃/ZnO nanocomposites exhibited a robust crystallinity and a high adsorption of dye molecules when compared to SiO₂@ZnO and SiO₂@ α -Fe₂O₃ nanocomposites, respectively. The experimental results demonstrated a rapid Methylene Blue (MB) degradation among these catalysts within short intervals of time with the addition of α -Fe₂O₃/ZnO mixed metal oxide catalysts on the SiO₂ nanospheres. Finally, a photo-Fenton reaction was implemented to confirm the presence of the hydroxyl (OH) radicals, which are powerful agents used for the degradation of organic pollutants.

Keywords: photo-Fenton reaction; nanocomposites; photocatalytic activity; degradation

1. Introduction

In order to avoid damage to the environment from greenhouse gases, it is necessary to develop renewable energy resources as alternatives to fossil fuels. Solar energy has received much attention as a sustainable and clean energy source. The conversion of solar energy into chemical energy is a promising technique in producing renewable energy [1]. It has also been found that photocatalysis can play a very effective role in removing organic pollutants from water [2]. Recently, semiconductor photocatalysis has been studied, especially for photocatalytic reactions, having a wide band gap acting as a UV and visible light photocatalyst [3]. Several researchers have focused on improving the conductivity and optical properties of heterogeneous semiconductor nanocomposite materials, particularly metal oxides. These are dominant because of their properties that enhance the surface plasmon effect and offer improvement in the visible light region [4].

Improved visible light photocatalysts grown from heterogeneous metal oxide semiconductor nanocomposites are expected to be suitable for a variety of applications [5]. In particular, these metal oxides have shown greater stability and sensitivity, especially for the degradation of organic pollutants [6]. Among the various metal oxides, ZnO and α -Fe₂O₃ are the best combination for the production of the heterogeneous photocatalysts used for wastewater treatment [7], CO₂ reduction [8], hydrogen production [9], CO oxidation [10], and water splitting [9,11]. The heterogeneous semiconductors can also be utilized to trap electrons at surface sites and to support the formation of superoxide anion radicals O₂^{•−} from O₂ molecules. There are many methods which can be used for the preparation of heterogeneous metal oxide nanocomposites, including hydrothermal [12], chemical

vapor deposition [13], sonochemical [14], and the sol-gel [15,16] method. Among these, the sol-gel method has several advantages, being more economical, requiring only a simple preparation, and having good stability and reproducibility [17].

In this work, $\text{SiO}_2@ \alpha\text{-Fe}_2\text{O}_3/\text{ZnO}$ metal oxide nanocomposites were utilized for the effective degradation of organic pollutants. Additionally, the introduction of ZnO nanoparticles onto the $\text{SiO}_2@ \alpha\text{-Fe}_2\text{O}_3$ nanocomposites offered the benefits of charge separation followed by the scavenging of electrons and holes by the surface adsorbed species, which consequently enhanced the degradation of the Methylene Blue (MB) dye. Furthermore, the addition of hydrogen peroxide (H_2O_2) improved the number of OH radicals and encouraged the degradation mechanism based on the photo-Fenton reaction. The two metal oxides $\alpha\text{-Fe}_2\text{O}_3$ and ZnO were grown on SiO_2 nanospheres to enhance the stability of the photocatalytic degradation.

2. Results and Discussion

2.1. X-ray Diffraction (XRD)

The XRD profiles of the as-prepared samples are shown in Figure 1. The diffraction peaks at 33.2° , 35.6° , and 40.9° are attributed to the 001, 101, and 002 planes (JCPDS no. 89-8104) of $\alpha\text{-Fe}_2\text{O}_3$, respectively, with the weak intensity being due to the very thin layer of $\alpha\text{-Fe}_2\text{O}_3$ [18]. In addition, the relatively broad peak observed at 24.5° , which arose from the SiO_2 , confirms that the deposition of $\alpha\text{-Fe}_2\text{O}_3$ occurred on the top of the SiO_2 spheres. Furthermore, the addition of ZnO to the SiO_2 spheres is shown by the 2θ peaks at 31.6° , 34.3° , 36.2° , 47.4° , and 56.6° that are ascribed to the 100, 002, 101, 102, and 110 planes, respectively (JCPDS 01-089-0510), indexed to the crystalline planes of the ZnO nanoparticles [19]. The existence of these 2θ peaks from the as-prepared samples confirms the presence of ZnO on the $\alpha\text{-Fe}_2\text{O}_3$ nanoparticles.

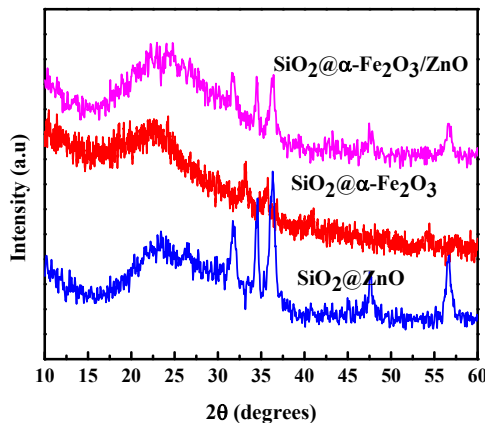


Figure 1. X-ray diffraction (XRD) pattern of $\text{SiO}_2@ \text{ZnO}$, $\text{SiO}_2@ \alpha\text{-Fe}_2\text{O}_3$ and $\text{SiO}_2@ \alpha\text{-Fe}_2\text{O}_3/\text{ZnO}$ nanocomposites.

2.2. Structural Properties

Figure 2a–c show Field emission scanning electron microscopy (FESEM) images of the $\text{SiO}_2@ \alpha\text{-Fe}_2\text{O}_3$, $\text{SiO}_2@ \text{ZnO}$, and $\text{SiO}_2@ \alpha\text{-Fe}_2\text{O}_3/\text{ZnO}$ nanocomposites. The SiO_2 nanospheres are uniform in size with smooth surfaces, as shown in Figure 2a. After the addition of $\alpha\text{-Fe}_2\text{O}_3$ on the SiO_2 , the surface becomes rough but still maintains the nanosphere structure even after annealing at 450°C . The uniform size distribution of the 40 nm ZnO nanoparticles observed on $\alpha\text{-Fe}_2\text{O}_3$ after the deposition of ZnO nanoparticles is shown in Figure 2c. It should be noted that the addition of two metal oxides onto SiO_2 does not change the shape of the nanospheres. This proves that the SiO_2 contains active sites for adsorbing any nanoparticle, leading to the improvement of the surface area of

the semiconductor nanoparticles. The atomic percentage of elements present in the nanocomposites, as observed by energy dispersive X-ray spectroscopy (EDX), are shown in Figure 2d.

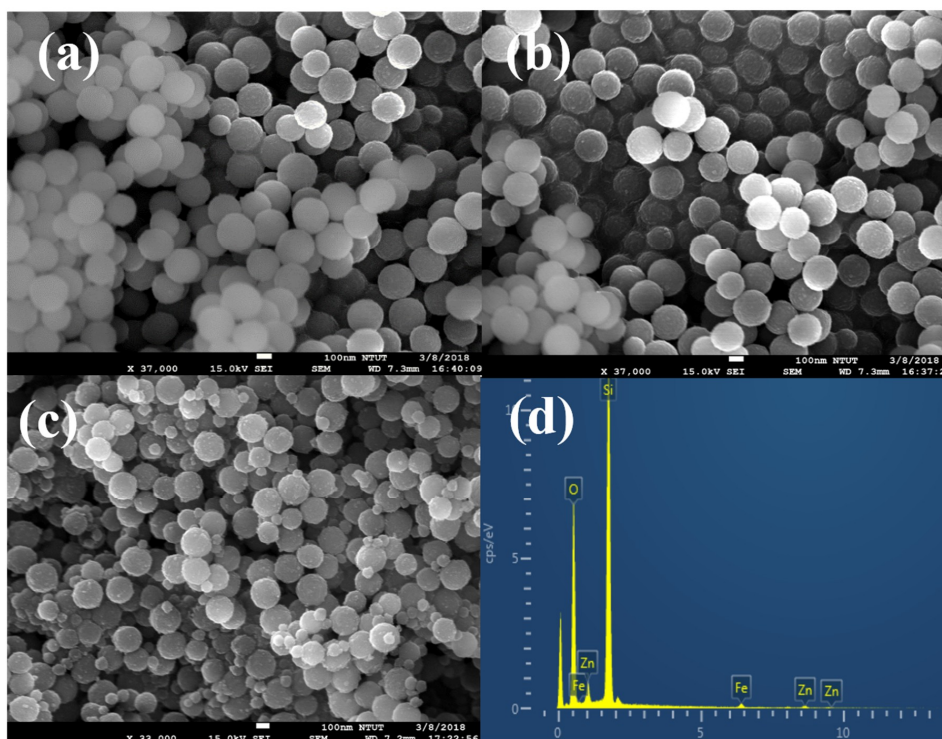


Figure 2. FESEM images of (a) SiO₂@ZnO, (b) SiO₂@α-Fe₂O₃ and (c) SiO₂@α-Fe₂O₃/ZnO nanocomposites. (d) Energy dispersive X-ray spectroscopy (EDX) analysis of SiO₂@α-Fe₂O₃/ZnO nanocomposites.

2.3. Fourier Transform Infrared Spectroscopy (FTIR) Analysis

Figure 3 shows the FTIR analysis of the SiO₂@α-Fe₂O₃, SiO₂@ZnO, and SiO₂@α-Fe₂O₃/ZnO nanocomposites. The peak at 1091 cm^{−1} shows the vibration structure of the Si–O–Si, which is observed in all of the spectra [20]. Moreover, there is a sharp peak observed at 1800 cm^{−1} shown in figure, revealing the stretching frequency of the Fe–O, and all of the metal oxides exhibit an OH group at 3500 cm^{−1} [21].

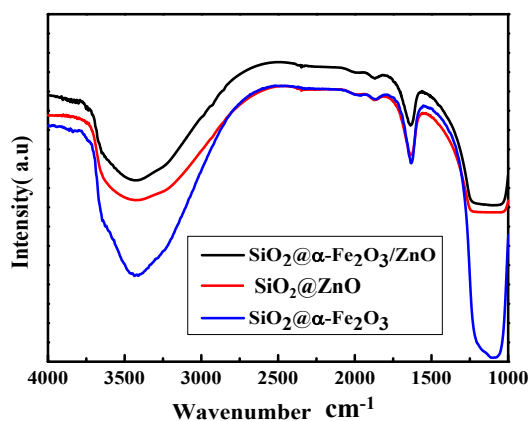


Figure 3. FTIR spectra of SiO₂@ZnO, SiO₂@α-Fe₂O₃ and SiO₂@α-Fe₂O₃/ZnO nanocomposites.

2.4. Optical Measurement

Figure 4 shows the UV–vis spectra of the $\text{SiO}_2@\text{ZnO}$, $\text{SiO}_2@\alpha\text{-Fe}_2\text{O}_3$, and $\text{SiO}_2@\alpha\text{-Fe}_2\text{O}_3/\text{ZnO}$ nanocomposites. From Figure 4, we can observe that the position of the absorption band of all of the nanocomposites in the visible region is between 400 and 900 nm. For the $\text{SiO}_2@\text{ZnO}$ nanocomposites, the absorption band observed at 340 nm confirms the formation of ZnO nanoparticles on the SiO_2 nanospheres [22]. For the $\text{SiO}_2@\alpha\text{-Fe}_2\text{O}_3$ nanocomposites, the absorption band appears at 320 and 540 nm for the $\alpha\text{-Fe}_2\text{O}_3$ on SiO_2 nanospheres. After the deposition of ZnO metal oxide on the $\text{SiO}_2@\alpha\text{-Fe}_2\text{O}_3$ nanocomposites, there is a broad absorption that extends to the visible region as compared to the $\text{SiO}_2@\text{ZnO}$ and $\text{SiO}_2@\alpha\text{-Fe}_2\text{O}_3$ nanocomposites.

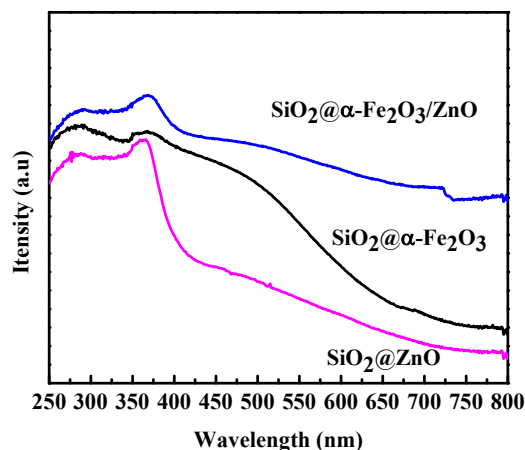


Figure 4. UV–vis spectra of $\text{SiO}_2@\text{ZnO}$, $\text{SiO}_2@\alpha\text{-Fe}_2\text{O}_3$ and $\text{SiO}_2@\alpha\text{-Fe}_2\text{O}_3/\text{ZnO}$ nanocomposites.

2.5. Photoluminescence (PL) Measurements

Figure 5 shows the PL spectra of the $\text{SiO}_2@\text{ZnO}$, $\text{SiO}_2@\alpha\text{-Fe}_2\text{O}_3$, and $\text{SiO}_2@\alpha\text{-Fe}_2\text{O}_3/\text{ZnO}$ nanocomposites. The PL signal is used to demonstrate the charge separation which results from the recombination of photoinduced carriers [23]. The intensities observed for the $\text{SiO}_2@\alpha\text{-Fe}_2\text{O}_3/\text{ZnO}$ nanocomposites are weak and thus indicative of better photocatalytic performance. Further higher intensity leads to a high electron-hole recombination which reduces the catalytic activity.

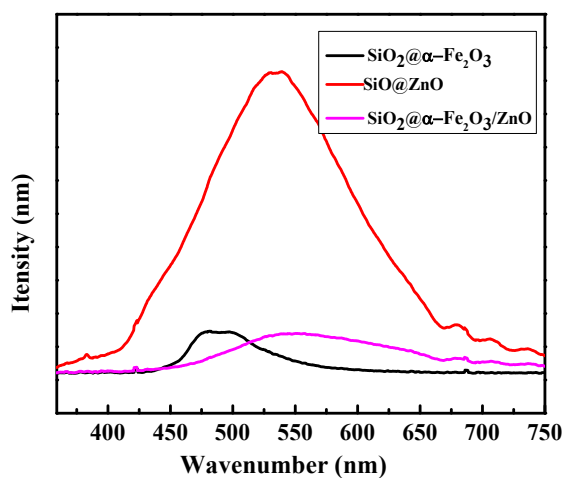


Figure 5. Photoluminescence (PL) spectra of $\text{SiO}_2@\text{ZnO}$, $\text{SiO}_2@\alpha\text{-Fe}_2\text{O}_3$ and $\text{SiO}_2@\alpha\text{-Fe}_2\text{O}_3/\text{ZnO}$.

2.6. Brunauer-Emmett-Teller (BET)-N₂ Adsorption-Desorption Analysis

A BET N₂ adsorption-desorption analysis was carried out to measure the specific surface area and porosity of as-synthesized materials. The BET surface areas of the as-prepared SiO₂, SiO₂@α-Fe₂O₃, SiO₂@ZnO, and SiO₂@α-Fe₂O₃/ZnO nanocomposites are 8, 21, 33 and 41 m²/g, respectively, as shown in Table 1. The pore volume of SiO₂@α-Fe₂O₃/ZnO nanocomposites is 0.51 cm³/g, which indicates the presence of a mesoporous structure. In this respect it could be helpful to enhance the catalytic activity. The surface areas of SiO₂@α-Fe₂O₃ and SiO₂@α-Fe₂O₃/ZnO nanocomposites spheres are higher than that of SiO₂ spheres. Finally, the addition of ZnO nanoparticles onto the SiO₂@α-Fe₂O₃ increased the size, surface area, and pore volume of the SiO₂@α-Fe₂O₃/ZnO nanocomposites, which suggests a possible advantage that could lead to increased photocatalytic activity.

Table 1. BET surface area of as-prepared SiO₂, SiO₂@α-Fe₂O₃, SiO₂@ZnO and SiO₂@α-Fe₂O₃/ZnO nanocomposites.

Samples	BET Surface Area	Pore Volume
SiO ₂	8 m ² /g	0.032 cm ³ /g
SiO ₂ @α-Fe ₂ O ₃	21 m ² /g	0.041 cm ³ /g
SiO ₂ @ZnO	33 m ² /g	0.045 cm ³ /g
SiO ₂ @α-Fe ₂ O ₃ /ZnO	41 m ² /g	0.051 cm ³ /g

3. Photocatalytic Activity

Figure 6a shows the photodegradation of MB dye which occurred with the SiO₂@α-Fe₂O₃/ZnO nanocomposites under visible light. The UV-vis spectrum of the MB dye showed two absorption peaks at 620 nm and 664 nm. The peak intensities of 620 and 664 nm decreased with an increasing irradiation time, indicating the degradation of MB dye. The percentage of MB dye remaining in the reaction medium using SiO₂@ZnO, SiO₂@Fe₂O₃ and SiO₂@α-Fe₂O₃/ZnO nanocomposites without H₂O₂ is shown in Figure 6b. The degradation percentage of the MB dye obtained using SiO₂@ZnO nanocomposites was 62% within 40 min without H₂O₂. When the H₂O₂ was added to the dye solution, the degradation percentage increased to 91%. Similar results were observed for the SiO₂@α-Fe₂O₃ nanocomposites with and without H₂O₂, giving a degradation efficiency towards MB dye of 42% and 82%, respectively, within 40 min. For the SiO₂@α-Fe₂O₃/ZnO mixed metal oxide catalyst, 100% degradation was achieved within 25 min with H₂O₂, whereas 96% degradation was observed at 40 min without H₂O₂.

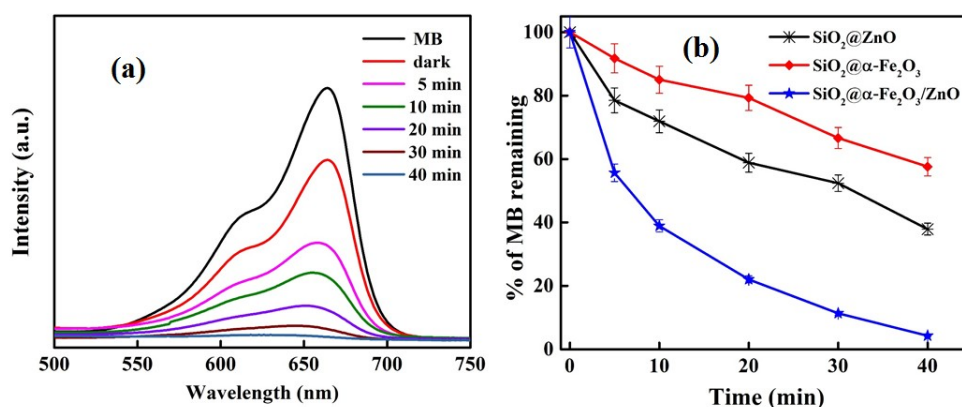


Figure 6. (a) Degradation of Methylene Blue MB dye (5 ppm) in the presence of SiO₂@α-Fe₂O₃/ZnO nanocomposites under visible light irradiation. (b) The plot shows the percentage of MB remaining vs. time.

Figure 7b shows the photo-Fenton and photocatalytic degradation reactions of the MB following the pseudo-first-order kinetics, termed as $\ln(C/C_0) = k't$, where k' is the rate constant. The rate constant increased with the addition of H_2O_2 , mainly due to the photo-Fenton activity. Based on these results, the $SiO_2@ \alpha\text{-Fe}_2O_3/ZnO + H_2O_2$ catalyst exhibits the highest rate constant ($k' = 1.69 \times 10^{-1} \text{ min}^{-1}$), which is 2.2 times higher than that of $SiO_2@ \alpha\text{-Fe}_2O_3/ZnO$ ($k' = 7.38 \times 10^{-2} \text{ min}^{-1}$) as well as 7.8 and 2.9 times greater than those of $SiO_2@ZnO$ ($k' = 2.16 \times 10^{-2} \text{ min}^{-1}$) and $SiO_2@ZnO + H_2O_2$ ($k' = 5.67 \times 10^{-2} \text{ min}^{-1}$), respectively. When compared to $SiO_2@ \alpha\text{-Fe}_2O_3$ ($k' = 1.328 \times 10^{-2} \text{ min}^{-1}$) and $SiO_2@ \alpha\text{-Fe}_2O_3 + H_2O_2$ ($k' = 4.18 \times 10^{-2} \text{ min}^{-1}$), the k' values are 12.7 and 4 times less than that of the $SiO_2@ \alpha\text{-Fe}_2O_3/ZnO + H_2O_2$ catalyst. Figure 7b shows the plot of $\ln(C/C_0)$ vs. time. Table 2 shows the statistical analysis of pseudo-first-order kinetics with respect to the rate constant (k') and correlation coefficient (R^2). For the photocatalytic degradation reaction, the R^2 values of $SiO_2@ZnO$, $SiO_2@ \alpha\text{-Fe}_2O_3$, and $SiO_2@ \alpha\text{-Fe}_2O_3/ZnO$ are almost equal to 1 (i.e., 0.9843, 0.9939 and 0.9948, respectively). Similarly, the photo-Fenton degradation exhibits R^2 values of 0.9932, 0.9727 and 0.9797, respectively. Both reactions show an almost linear decrease in the concentration, which confirms the photocatalysis on the pseudo-first-order kinetics mechanism.

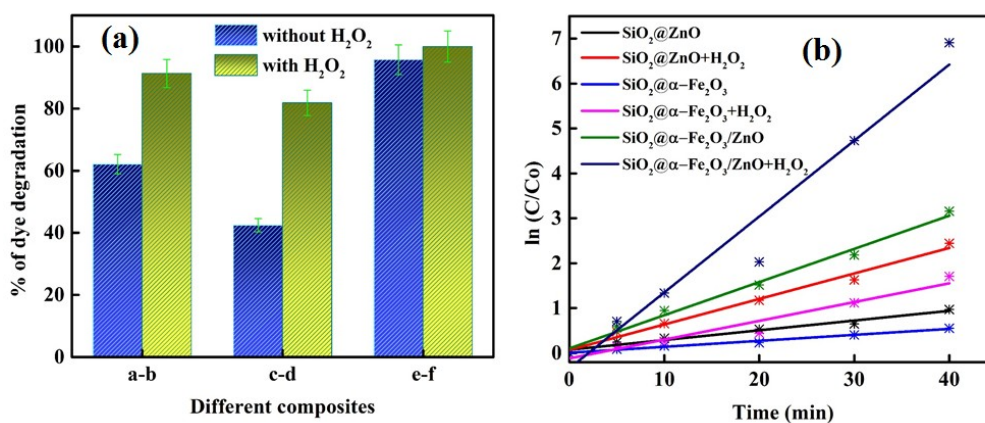


Figure 7. (a) Photo-Fenton degradation of MB using different nanocomposites with and without H_2O_2 : letter a— $SiO_2@ZnO$, letter b— $SiO_2@ZnO + H_2O_2$, letter c— $SiO_2@ \alpha\text{-Fe}_2O_3$, letter d— $SiO_2@ \alpha\text{-Fe}_2O_3 + H_2O_2$, letter e— $SiO_2@ \alpha\text{-Fe}_2O_3/ZnO$, letter f— $SiO_2@ \alpha\text{-Fe}_2O_3/ZnO + H_2O_2$. (b) The plot of $\ln(C/C_0)$ vs. time.

Table 2. Statistical analysis of pseudo-first-order kinetics for photocatalytic and photo-Fenton degradation reactions towards MB.

Samples	r_0	$k' \text{ (min}^{-1}\text{)}$	R^2	T (min)	% D_{eg}
$SiO_2@ZnO$	0.0067	0.0216	0.9843	40	62
$SiO_2@ZnO + H_2O_2$	0.0177	0.0567	0.9932	40	91
$SiO_2@ \alpha\text{-Fe}_2O_3$	0.0041	0.0132	0.9939	40	42
$SiO_2@ \alpha\text{-Fe}_2O_3 + H_2O_2$	0.0130	0.0418	0.9727	40	82
$SiO_2@ \alpha\text{-Fe}_2O_3/ZnO$	0.0230	0.0738	0.9948	40	96
$SiO_2@ \alpha\text{-Fe}_2O_3/ZnO + H_2O_2$	0.0527	0.1691	0.9797	25	100

r_0 —initial MB dye degradation rate ($r_0 = k' \times C_0$), k' —rate constant, R^2 —correlation coefficient for pseudo-first order, T—degradation time, % D_{eg} —percentage of degradation efficiency.

The photocatalytic reaction under visible light means that the semiconductor can be utilized to adsorb organic pollutants. Here, we can see that the active SiO_2 surface for the deposition of $\alpha\text{-Fe}_2O_3$ and ZnO metal oxides helped with the transport of photogenerated e^- and h^+ [24]. The mixed semiconductor nanoparticles have a larger surface area and greater light absorption harvesting which transports the dye molecules, thus enhancing the dye degradation. Furthermore, the conduction band (CB) of $\alpha\text{-Fe}_2O_3$ is slightly negative while the valance band (VB) is more positive than that of

ZnO. The transfer of holes from ZnO to α -Fe₂O₃ must be higher when compared with the individual metal oxides. This may be due to the efficient production of the charge carriers based on the strong interaction between the α -Fe₂O₃ and ZnO heterostructures, which reduces the photogenerated charge recombination rate, thus improving the photocatalytic activity [25]. In order to increase the holes in α -Fe₂O₃ and ZnO, H₂O₂ is used as an oxidizing agent to produce OH radicals. It reacts with water molecules in the dye solution and OH-groups present on the surface.

Figure 8 shows the PL spectra for the photodegradation of MB dye using SiO₂@ α -Fe₂O₃/ZnO nanocomposites in the presence of terephthalic acid at different time intervals under visible light irradiation. The PL intensity increases when increasing the reaction time due to the OH scavenger of terephthalic acid, which does not react with other radicals. These results confirm that the OH radicals were formed during the photo-Fenton reaction, leading to the MB dye degradation.

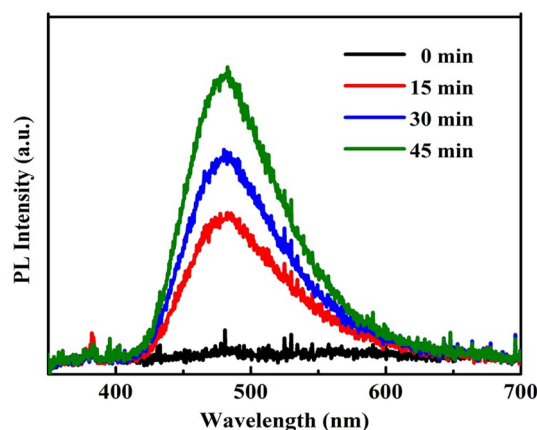


Figure 8. PL spectra for photodegradation of MB dye using SiO₂@ α -Fe₂O₃/ZnO nanocomposites in the presence of terephthalic acid at different time intervals under visible light irradiation.

The various reports on dye degradation match well with our study, and their results are compared as shown in Table 3. From Table 3, we can observe the low degradation time of 40 min for SiO₂@ α -Fe₂O₃/ZnO nanocomposites, as compared with previous reports [26–36]. Adding H₂O₂ to SiO₂@ α -Fe₂O₃/ZnO nanocomposites produces more electron-hole pairs, which leads to the faster degradation of MB dye, within 25 min. This shows a low degradation time when compared with other reports, as shown in the table below.

Table 3. Comparison of our work with the reported work.

Catalyst	Dye	Catalyst Loading	Time (min)	Reference
ZnO/CdO	MB	*R.a.—500 mL	360	[26]
Ce-doped SiO ₂ /TiO ₂	MB	100 mg—1000 mL	120	[27]
CoFe ₂ O ₄ —Cr ₂ O ₃ —SiO ₂	MB	20 mg—50 mL	120	[28]
ZnO	MB	1500 mg—650 mL	120	[29]
Fe ₃ O ₄ @SiO ₂ @ZnO	4NP	400 mg—30 mL	120	[30]
α -Fe ₂ O ₃ /ZnO	RhB	20 mg—40 mL	105	[31]
G-Fe ₂ O ₃ /ZnO	MB	10 mg—50 mL	90	[32]
(RGO)/ α -Fe ₂ O ₃	MB	100 mg—100 mL	90	[33]
Ag ₃ PO ₄ /Fe ₂ O ₃	MO	200 mg—25 mL	60	[34]
γ -Fe ₂ O ₃ /ZnO	MB	50 mg—100 mL	50	[35]
Fe/ZnO/SiO ₂	MB	75 mg—300 mL	30	[36]
SiO ₂ @ α -Fe ₂ O ₃ /ZnO	MB	50 mg—100 mL	40	This work
SiO ₂ @ α -Fe ₂ O ₃ /ZnO+H ₂ O ₂	MB	50 mg—100 mL	25	This work

MB—Methylene Blue, 4NP—4 Nitro Phenol, RhB—Rhodamine B, MO—Methylene Orange, *R.a.—required amount.

4. Experimental Procedure

For the preparation of the nanocomposites, SiO₂ nanospheres were first prepared as per our previous work [10]. The SiO₂ spheres were synthesized from a mixture of tetraethyl orthosilicate (TEOS), anhydrous ethanol, and water, which was stirred at room temperature for 15 min. After this, an ammonia and anhydrous ethanol solution were added to the mixture and it was stirred for 8 h. The resulting product of SiO₂ spheres was kept in a vacuum oven at 60 °C for 6 h. Further, for the synthesis of the mixed metal oxides, iron (III) nitrate monohydrate and zinc acetate precursors were used. The SiO₂ spheres were uniformly dispersed in 40 mL water by ultrasonication, followed by the addition of iron(III) chloride hexahydrate and urea with effective stirring at 90 °C for 10 h. The prepared FeOOH-coated SiO₂ spheres were washed with water and ethanol. Subsequently, FeOOH-coated SiO₂ spheres were dispersed in water followed by adding zinc acetate dihydrate and NaOH with effective stirring at 100 °C for 6 h. SiO₂@ α -Fe₂O₃/ZnO nanocomposites were separated by centrifugation and washed with ethanol and water. The above cleaning procedure was repeated three times and the resultant product was then annealed at 450 °C for 2 h to produce a crystalline substance. For the purpose of comparison, both SiO₂@ α -Fe₂O₃ and SiO₂@ZnO samples were prepared using the above procedure.

Photocatalytic Reaction

The photocatalytic degradation reaction of MB dye was carried out using metal oxide nanocomposites in the presence of visible light irradiation using a 350 W Mercury-Xenon lamp, (Prosper Optoelectronics, Taiwan) for which the intensity of light at 380–780 nm was 0.33 mW·cm^{−2}. In order to attain an adsorption-desorption equilibrium between the catalyst surface and dye molecules, the mixed metal oxide nanocomposite catalysts (50 mg) were mixed with 5 ppm of 100 mL MB dye solution. Initially, the dye was stirred for 10 min in the dark. Following this, we introduced the visible light. The same procedure as that mentioned above was followed to carry out photo-Fenton experiments. Additionally, 0.1 mL of H₂O₂ was added as an initial step. Every 10 min, 5 mL of the solution was taken and measured with a UV–vis spectrum to confirm the degradation.

5. Characterization

The XRD spectra were recorded using an X-ray diffractometer (XRD, PAN analytical X' Pert PRO, Almelo, The Netherlands). FESEM images were obtained using a JEOL (JSM-7610F, Tokyo, Japan) microscope at an operating voltage of 15 kV. The sample was coated with platinum for effective imaging before being charged. UV–vis DRS were recorded using a UV–vis spectrophotometer (Cary 5000, Santa Clara, CA, USA). The prepared nanocomposites of the chemical structure were studied using a PerkinElmer FTIR spectrometer. The surface area of the samples was measured via N₂ adsorption-desorption isotherms at 77 K (BET, Micromeritics ASAP 2020, Norcross, GA, USA). PL studies were observed using a PL spectrometer (Dongwoo-Ramboss 500i, Gyeonggi-Do, Korea).

6. Conclusions

In summary, we successfully prepared SiO₂@ α -Fe₂O₃/ZnO nanocomposites using a cost-effective sol-gel method. The improved performance of dye degradation through the addition of metal oxides is attributed to the fast carrier charge that reduced the electron-hole pair recombination. From the results, it is proven that SiO₂@ α -Fe₂O₃/ZnO nanocomposites were able to degrade the MB dye within 25 min after adding a reducing agent. Furthermore, ZnO exhibits strong interactions between the bridging oxygen on the surface of α -Fe₂O₃ and allows the photo-oxidation decomposition of pollutants. In order to enhance the photo-Fenton activity, H₂O₂ was added to the dye solution, which helped to increase the number of ·OH groups. When H₂O₂ is added to the dye solution, the SiO₂@ α -Fe₂O₃/ZnO catalyst can increase the visible light stability and yield a faster separation of photogenerated electrons and holes. These behaviors are favorable for the faster degradation of MB dye using SiO₂@ α -Fe₂O₃/ZnO catalyst.

Author Contributions: K.U. and T.C.-K.Y. conceived and designed the experiments; S.B. performed XRD, PL, and FTIR experiments; results were discussed with the assistance of G.-T.P.; and K.U. wrote the paper with the assistance of S.B.

Funding: This research received no external funding.

Acknowledgments: The authors are grateful to the Precision Analysis and Materials Research Center, National Taipei University of Technology, Taipei, for their financial support.

Conflicts of Interest: The authors declare no conflict of interest.

References

1. Crespo, C.T. CuNbO_3 as a solar energy converter to fuel and electricity. *Sol. Energy Mater. Sol. Cells* **2018**, *179*, 305–311. [[CrossRef](#)]
2. Qing, W.; Chen, K.; Wang, Y.; Liu, X.; Lu, M. Green synthesis of silver nanoparticles by waste tea extract and degradation of organic dye in the absence and presence of H_2O_2 . *Appl. Surf. Sci.* **2017**, *423*, 1019–1024. [[CrossRef](#)]
3. Xie, J.; Zhou, Z.; Lian, Y.; Hao, Y.; Li, P.; Wei, Y. Synthesis of $\alpha\text{-Fe}_2\text{O}_3/\text{ZnO}$ composites for photocatalytic degradation of pentachlorophenol under UV-vis light irradiation. *Ceram. Int.* **2015**, *41*, 2622–2625. [[CrossRef](#)]
4. Zhou, Y.; Li, J.; Liu, C.; Huo, P.; Wang, H. Construction of 3D porous $\text{g-C}_3\text{N}_4/\text{AgBr}/\text{rGO}$ composite for excellent visible light photocatalytic activity. *Appl. Surf. Sci.* **2018**, *458*, 586–596. [[CrossRef](#)]
5. Zhou, K.; Hu, X.Y.; Chen, B.Y.; Hsueh, C.C.; Zhang, Q.; Wang, J.; Lin, Y.J.; Chang, C.T. Synthesized $\text{TiO}_2/\text{ZSM-5}$ composites used for the photocatalytic degradation of azo dye: Intermediates, reaction pathway, mechanism and bio-toxicity. *Appl. Surf. Sci.* **2016**, *383*, 300–309. [[CrossRef](#)]
6. Mahadik, M.A.; An, G.W.; David, S.; Choi, S.H.; Cho, M.; Jang, J.S. Fabrication of A/R- TiO_2 composite for enhanced photoelectrochemical performance: Solar hydrogen generation and dye degradation. *Appl. Surf. Sci.* **2017**, *426*, 833–843. [[CrossRef](#)]
7. Wachs, I.E.; Routray, K. Catalysis science of bulk mixed oxides. *ACS Catal.* **2012**, *2*, 1235–1246. [[CrossRef](#)]
8. Geng, Z.G.; Kong, X.D.; Chen, W.W.; Su, H.Y.; Liu, Y.; Cai, F.; Wang, G.X.; Zeng, J. Oxygen Vacancies in ZnO Nanosheets Enhance CO_2 Electrochemical Reduction to CO. *Angew. Chem. Int. Ed.* **2018**, *57*, 6054–6059. [[CrossRef](#)] [[PubMed](#)]
9. Boudjemaa, A.; Trari, M. Photo-catalytic hydrogen production over Fe_2O_3 based catalysts. *Int. J. Hydrogen Energy* **2010**, *35*, 7684–7689. [[CrossRef](#)]
10. Uma, K.; Chen, S.W.; Arjun, N.; Pan, G.T.; Yang, T.C.K. The production of an efficient visible light photocatalyst for CO oxidation through the surface plasmonic effect of Ag nanoparticles on $\text{SiO}_2/\alpha\text{-Fe}_2\text{O}_3$ nanocomposites. *RSC Adv.* **2018**, *8*, 12547–12555. [[CrossRef](#)]
11. Lv, R.; Wang, T.; Su, F.; Zhang, P.; Li, C.; Gong, J. Facile synthesis of ZnO nanopencil arrays for photoelectrochemical water splitting. *Nano Energy* **2014**, *7*, 143–150. [[CrossRef](#)]
12. Tao, Q.; Chen, M.; He, H.; Komarneni, S. Hydrothermal transformation of mixed metal oxides and silicate anions to phyllosilicate under highly alkaline conditions. *Appl. Clay Sci.* **2018**, *156*, 224–230. [[CrossRef](#)]
13. Voznyi, A.; Kosyak, V.; Opanasyuk, A.; Tirkusova, N.; Grase, L.; Medvids, A.; Mezinskis, G. Structural and electrical properties of SnS_2 thin films. *Mater. Chem. Phys.* **2016**, *173*, 52–61. [[CrossRef](#)]
14. Yan, K.L.; Shang, X.; Li, Z.; Dong, B.; Li, X.; Gao, W.K.; Chi, J.Q.; Chai, Y.M.; Liu, C.G. Ternary mixed metal Fe-doped NiCo_2O_4 nanowires as efficient electrocatalysts for oxygen evolution reaction. *Appl. Surf. Sci.* **2017**, *416*, 371–378. [[CrossRef](#)]
15. Al-Owais, A.A. Synthesis and magnetic properties of hexagonally packed ZnO nanorods. *Arab. J. Chem.* **2013**, *6*, 229–234. [[CrossRef](#)]
16. Millar, A.; Rahman, M.M.; Jiang, Z.T. Review of sol-gel derived mixed metal oxide thin film coatings with the addition of carbon materials for selective surface applications. *J. Adv. Phys.* **2014**, *3*, 179–193. [[CrossRef](#)]
17. Perdomo, C.; Pérez, A.; Molina, R.; Moreno, S. Storage capacity and oxygen mobility in mixed oxides from transition metals promoted by cerium. *Appl. Surf. Sci.* **2016**, *383*, 42–48. [[CrossRef](#)]
18. Balu, S.; Uma, K.; Pan, G.T.; Yang, T.; Ramaraj, S. Degradation of methylene blue dye in the presence of visible light using $\text{SiO}_2/\alpha\text{-Fe}_2\text{O}_3$ nanocomposites deposited on SnS_2 flowers. *Materials* **2018**, *11*, 1030. [[CrossRef](#)] [[PubMed](#)]

19. Bindu, P.; Thomas, S. Estimation of lattice strain in ZnO nanoparticles: X-ray peak profile analysis. *J. Theor. Appl. Phys.* **2014**, *8*, 123–134. [[CrossRef](#)]
20. Uma, K.; Arjun, N.; Pan, G.T.; Yang, T.C.K. The photodeposition of surface plasmon Ag metal on SiO₂@ α -Fe₂O₃ nanocomposites sphere for enhancement of the photo-fenton behavior. *Appl. Surf. Sci.* **2017**, *425*, 377–383. [[CrossRef](#)]
21. Xu, W.; Wang, H.; Liu, R.; Zhao, X.; Qu, J. The mechanism of antimony(III) removal and its reactions on the surfaces of Fe–Mn binary oxide. *J. Colloid Interface Sci.* **2011**, *363*, 320–326. [[CrossRef](#)] [[PubMed](#)]
22. Segets, D.; Gradl, J.; Taylor, R.K.; Vassilev, V.; Peukert, W. Analysis of optical absorbance spectra for the determination of ZnO nanoparticle size distribution, solubility, and surface energy. *ACS Nano* **2009**, *3*, 1703–1710. [[CrossRef](#)] [[PubMed](#)]
23. Feng, Y.; Zhou, Y.; Liu, Y.; Zhang, G.; Zhang, X. Photoluminescence spectra of nano-structured ZnO thin films. *J. Lumin.* **2006**, *119–120*, 233–236. [[CrossRef](#)]
24. Quintana, M.; Edvinsson, T.; Hagfeldt, A.; Boschloo, G. Comparison of dye-sensitized ZnO and TiO₂ solar cells: Studies of charge transport and carrier lifetime. *J. Phys. Chem. C* **2007**, *111*, 1035–1041. [[CrossRef](#)]
25. Xie, J.; Zhang, L.; Li, M.; Hao, Y.; Lian, Y.; Li, Z.; Wei, Y. A-Fe₂O₃ modified ZnO flower-like microstructures with enhanced photocatalytic performance for pentachlorophenol degradation. *Ceram. Int.* **2015**, *41*, 9420–9425. [[CrossRef](#)]
26. Saravanan, R.; Shankar, H.; Prakash, T.; Narayanan, V.; Stephen, A. ZnO/CdO composite nanorods for photocatalytic degradation of methylene blue under visible light. *Mater. Chem. Phys.* **2011**, *125*, 277–280. [[CrossRef](#)]
27. Liu, Y.; Yu, H.; Lv, Z.; Zhan, S.; Yang, J.; Peng, X.; Ren, Y.; Wu, X. Simulated-sunlight-activated photocatalysis of methylene blue using cerium-doped SiO₂/TiO₂ nanostructured fibers. *J. Environ. Sci.* **2012**, *24*, 1867–1875. [[CrossRef](#)]
28. Senapati, K.K.; Borgohain, C.; Sarma, K.C.; Phukan, P. Photocatalytic degradation of methylene blue in water using CoFe₂O₄–Cr₂O₃–SiO₂ fluorescent magnetic nanocomposite. *J. Mol. Catal. A Chem.* **2011**, *346*, 111–116. [[CrossRef](#)]
29. Jang, Y.J.; Simer, C.; Ohm, T. Comparison of zinc oxide nanoparticles and its nano-crystalline particles on the photocatalytic degradation of methylene blue. *Mater. Res. Bull.* **2006**, *41*, 67–77. [[CrossRef](#)]
30. Qin, Y.; Zhang, H.; Tong, Z.; Song, Z.; Chen, N. A facile synthesis of Fe₃O₄@SiO₂@ZnO with superior photocatalytic performance of 4-nitrophenol. *J. Environ. Chem. Eng.* **2017**, *5*, 2207–2213. [[CrossRef](#)]
31. Wu, W.; Zhang, S.; Xiao, X.; Zhou, J.; Ren, F.; Sun, L.; Jiang, C. Controllable synthesis, magnetic properties, and enhanced photocatalytic activity of spindle-like mesoporous α -Fe₂O₃/ZnO core-shell heterostructures. *ACS Appl. Mater. Interfaces* **2012**, *4*, 3602–3609. [[CrossRef](#)] [[PubMed](#)]
32. Kumar, S.V.; Huang, N.; Yusoff, N.; Lim, H. High performance magnetically separable graphene/zinc oxide nanocomposite. *Mater. Lett.* **2013**, *93*, 411–414. [[CrossRef](#)]
33. Muthukrishnaraj, A.; Vadivel, S.; Kamalakannan, V.; Balasubramanian, N. α -Fe₂O₃/reduced graphene oxide nanorod as efficient photocatalyst for methylene blue degradation. *Mater. Res. Innov.* **2015**, *19*, 258–264. [[CrossRef](#)]
34. Yan, Y.; Guan, H.; Liu, S.; Jiang, R. Ag₃PO₄/Fe₂O₃ composite photocatalysts with an *n–n* heterojunction semiconductor structure under visible-light irradiation. *Ceram. Int.* **2014**, *40*, 9095–9100. [[CrossRef](#)]
35. Liu, Y.; Yu, L.; Hu, Y.; Guo, C.; Zhang, F.; Lou, X.W.D. A magnetically separable photocatalyst based on nest-like γ -Fe₂O₃/ZnO double-shelled hollow structures with enhanced photocatalytic activity. *Nanoscale* **2012**, *4*, 183–187. [[CrossRef](#)] [[PubMed](#)]
36. Mohamed, R.; Mkhallid, I.; Baeissa, E.; Al-Rayyani, M. Photocatalytic degradation of methylene blue by Fe/ZnO/SiO₂ nanoparticles under visiblelight. *J. Nanotechnol.* **2012**, *2012*. [[CrossRef](#)]

